Applied Catalysis B: Environmental 142–143 (2013) 54–64

Contents lists available at SciVerse ScienceDirect

Applied Catalysis B: Environmental

journal homepage: www.elsevier.com/locate/apcatb

Total oxidation of dichloromethane and ethanol over ceria–zirconia mixed oxide supported platinum and gold catalysts

Lenka Matějová[a,*], Pavel Topka[a], Luděk Kaluža[a], Satu Pitkäaho[b], Satu Ojala[b], Jana Gaálová[a], Riitta L. Keiski[b]

[a] Institute of Chemical Process Fundamentals of the ASCR, v.v.i., Rozvojová 135, 165 02 Praha 6, Czech Republic
[b] Department of Process and Environmental Engineering, University of Oulu, P.O. Box 4300, 90014 Oulu, Finland

ARTICLE INFO

Article history:
Received 5 December 2012
Received in revised form 26 April 2013
Accepted 30 April 2013
Available online 8 May 2013

Keywords:
Gold
Platinum
Ceria
Zirconia
VOC oxidation

ABSTRACT

$Ce_{0.5}Zr_{0.5}O_2$ prepared by sol–gel method was used as a support for platinum and gold catalysts that were tested in total oxidation of dichloromethane and ethanol. It was shown that the deposition of platinum and gold on $Ce_{0.5}Zr_{0.5}O_2$ support enhanced the reducibility of surface ceria. This phenomenon was more pronounced for platinum catalysts. Introduction of both noble metals led to the decrease of catalysts' acidity. In total oxidation of dichloromethane, the noble metal catalysts showed lower catalytic performance compared to parent $Ce_{0.5}Zr_{0.5}O_2$, due to lower amount of acid sites that act as chemisorption sites for chlorinated compounds. On the other hand, platinum catalysts exhibited significantly enhanced selectivity to CO_2 in comparison with the $Ce_{0.5}Zr_{0.5}O_2$ support. In total oxidation of ethanol, the deposition of platinum on $Ce_{0.5}Zr_{0.5}O_2$ resulted in a significant increase in catalytic performance, while the introduction of gold had only a minor effect. Moreover, the positive effect of higher noble metal loading on catalytic performance was more pronounced for Pt catalysts. For all investigated catalysts, the temperature of the H_2-TPR peak corresponding to the reduction of surface ceria correlated with their catalytic performance. The influence of Pt loading on the mechanism of ethanol oxidation was revealed. Based on the concentration profiles of individual by-products/products detected by on-line FTIR analysis, the possible pathways of their formation were suggested. Both noble metal catalysts exhibited higher selectivity to CO_2 than the pristine $Ce_{0.5}Zr_{0.5}O_2$.

1. Introduction

Volatile organic compounds (VOCs) belong to the group of major air pollutants. They contribute to greenhouse effect, destroy stratospheric ozone and control the rate of oxidant formation during the production of ground-level ozone, which is the primary constituent of the photochemical smog [1,2]. Many of the VOCs are harmful to human health. They cause a variety of adverse health effects including sensory irritation symptoms, allergies, asthma, neurological and liver toxicity, and cancers [3].

The compounds used as model VOCs in this work are dichloromethane and ethanol. Dichloromethane belongs to the three most commonly used chlorinated solvents in Europe [4]. Nevertheless, it is an eye and skin irritating agent, which may have effects on the central nervous system and liver, and is considered as possibly carcinogenic to humans [5]. On the other hand, ethanol is nowadays extensively used as renewable and environmentally friendly component of biofuels. However, the combustion of ethanol in car engines yields significant amounts of formaldehyde and acetaldehyde, which are considered as carcinogens and contribute to the formation of ground-level ozone [6].

By now, the major contributor to VOC emissions in Europe has been solvent and product use, which has comprised of about 40% of total non-methane VOCs emissions. Even if the total emissions of VOCs have decreased about 50% during 1990–2008, still more efforts are needed to decrease the emissions, and especially those most dangerous such as chlorinated hydrocarbons [7]. Catalytic oxidation is already used in VOC emission treatment. It has proven to be cost-effective and environmentally friendly technology for the solvent-using industry [8]. However, since the emission limit values are getting smaller and smaller, more effective and durable catalysts are needed. In addition, even when the catalytic treatment technology exists for the most typical solvents, more detailed studies are needed when substituted organics are oxidized.

Typically used active phases of the catalysts for VOC oxidation are noble metals, since they are very active even at low metal loadings and they have good duration of life [9]. When substituted organic compounds are considered, the selectivity of the catalyst becomes very important. The formation of harmful by-products or/and over-oxidation (for example in the case

* Corresponding author. Tel.: +420 220 390 283; fax: +420 220 920 661.
E-mail address: matejova@icpf.cas.cz (L. Matějová).

0926-3373/$ – see front matter © 2013 Elsevier B.V. All rights reserved.
http://dx.doi.org/10.1016/j.apcatb.2013.04.069

of S-containing VOCs) has to be avoided. In the case of ethanol and dichloromethane, Pt-catalysts are often used [10,11]. This is why we have selected Pt as a comparison base for the novel gold-based catalysts. In contrast to Pt and Pd, Au is rather new catalytic material. Au catalysts have been investigated more for deep oxidation of VOCs since 1996 [12]. When it comes to support material, ceria–zirconia mixed oxides were only recently proposed as supports for the oxidation of VOCs [13,14]. They possess unique combination of elevated oxygen transport capacity coupled with ability to shift easily between reduced and oxidized state ($Ce^{3+} \leftrightarrow Ce^{4+}$), which induces a high refilling of active oxygen at catalyst surface and very good oxygen storage capacity. In the oxidation of 1,2-dichloroethane and trichloroethylene, ceria–zirconia mixed oxides were more active than the pure oxides. Their catalytic properties were found to depend on Ce/Zr molar content with $Ce_{0.5}Zr_{0.5}O_2$ showing the highest catalytic activity [13].

The aim of this study was to explore in detail the performance and selectivity of $Ce_{0.5}Zr_{0.5}O_2$ supported Au catalysts in dichloromethane and ethanol oxidation and to compare them with more conventional Pt catalyst supported on the same mixed oxide. Since ethanol oxidation over similar Au and Pt catalysts supported on ceria–zirconia mixed oxide was already investigated in the previous paper [15], the merit of the present article in regard to ethanol oxidation consists in a detailed study of the catalyst selectivity and the influence of low and high Pt and Au loadings on the distribution of ethanol oxidation by-products. The catalytic performance of Au and Pt catalysts in both oxidation reactions is discussed with respect to their physicochemical properties and compared with literature data.

2. Experimental

2.1. Catalyst preparation

$Ce_{0.5}Zr_{0.5}O_2$ support (labelled as CeZr) was prepared as follows: after dissolution of 38 g of zirconium *n*-propoxide (70 wt.% solution in propan-1-ol, Fluka, Prod. No. 96595) in 51 mL of propan-2-ol (Lach-Ner, Prod. No. 30470), the solution was added to the solution of 25 g of cerium(III) nitrate hexahydrate (Strem Chemicals, Prod. No. 93-5831) in 25 mL distilled water with a rate of 5 mL min^{-1} under vigorous stirring at ambient temperature. A pseudogel was formed immediately as the reactant hydrolyzed. The pseudogel was dried over a sand bath at 60 °C for 1 h. Then the sample was dried in an oven at 120 °C for 24 h and calcined in a batch furnace at 500 °C with a temperature ramp rate of 5 °C min^{-1} and dwell time 1 h at 300 °C and 5 h at 500 °C. The sample was then crushed and sieved to particle size fraction of 0.16–0.32 mm.

Three grams of the $Ce_{0.5}Zr_{0.5}O_2$ support was impregnated with 6 mL of aqueous solutions of either gold(III) acetate (Alfa Aesar, Prod. No. 39742) or platinum(II) tetraaminehydroxide (Alfa Aesar, Prod. No. 42918) as described elsewhere [15]. The impregnated sample was dried in an oven at 120 °C for 24 h and calcined in a batch furnace at 500 °C with a temperature ramp rate of 5 °C min^{-1} and dwell time 1 h at 300 °C and 5 h at 500 °C. The sample was then crushed and sieved to particle size fraction of 0.16–0.32 mm. The catalysts were labelled according to the actual contents of Au (0.3 and 2.8 wt.%) and Pt (0.2 and 1.5 wt.%) determined by chemical analysis as 0.3Au/CeZr, 2.8Au/CeZr, 0.2Pt/CeZr, and 1.5Pt/CeZr, respectively.

2.2. Catalyst characterization

The catalysts were characterized by atomic emission spectroscopy with inductively coupled plasma (ICP-AES), X-ray fluorescence spectroscopy (XRF), nitrogen physisorption, powder X-ray diffraction (XRD), temperature programmed reduction by hydrogen (H_2-TPR), temperature programmed desorption of ammonia (NH_3-TPD) and field-emission scanning electron microscopy (FE-SEM).

Chemical analysis of Au and Pt in catalysts was done using the Intrepid II DUO ICP-AES spectrometer (GBC). The concentration of elements was quantified in solutions obtained by decomposition of samples by melting in $KHSO_4$ in porcelain crucibles, filtration and dissolution in water.

X-ray fluorescence (XRF) analysis was performed with the ARL 9400 XP sequential WD-XRF spectrometer. The spectrometer was equipped with Rh anode end-window X-ray tube type 4GN fitted with 75 μm Be window. All peak intensity data were collected under vacuum conditions using the software WinXRF. The generator settings-collimator–crystal–detector combinations were optimized for all 79 measured elements with analysis time of 6 s per element. The obtained data were evaluated by standardless software Uniquant 4. The analysed powders were pressed into pellets about 5 mm thick and the diameter of 40 mm without any binding agent and covered with 4 μm supporting polypropylene film.

Nitrogen physisorption on catalyst powders (grain size 0.16–0.32 mm) was performed using ASAP 2020 Micromeritics instrument after degassing at 105 °C for 24 h under 1 Pa vacuum. The adsorption–desorption isotherms of nitrogen at −196 °C were treated by the standard Brunauer–Emmett–Teller (BET) procedure [16] for the p/p_0 range = 0.05–0.25 to calculate the specific surface area S_{BET}. The mesopore surface area, S_{meso}, and the micropore volume, V_{micro}, were determined by the *t*-plot method [17,18]. The total pore volume, V_{total}, was determined from nitrogen adsorption isotherm at maximum p/p_0 (~0.995). The pore-size distribution (pore radius 10^0–10^2 nm) was evaluated from the adsorption branch of the nitrogen adsorption–desorption isotherm by the Barrett–Joyner–Halenda (BJH) method [19] via the Roberts algorithm [20] assuming the cylindrical pore geometry. The Lecloux–Pirard standard isotherm [21] was employed for the *t*-plot as well as for the pore-size distribution evaluation.

The powder X-ray diffraction (XRD) data were collected with a PANalytical X'Pert PRO diffractometer in Bragg–Brentano reflecting geometry with fixed slits using Co Kα radiation. The patterns were acquired in the diffraction angle range 2Θ = 20–80° with a step size of 0.02 °. The crystallite-size was calculated according to the Scherrer equation [22].

The temperature-programmed reduction (TPR) measurements of catalysts (0.300 g) were performed with the H_2/N_2 mixture (10 mol.% H_2), flow rate 50 mL min^{-1} and linear temperature increase 20 °C min^{-1} up to 1000 °C. A change in H_2 concentration was detected with a mass spectrometer Omnistar 300 (Pfeiffer Vacuum). Reduction of the grained CuO (0.16–0.32 mm) was performed in each experiment to calculate the absolute values of hydrogen consumed during reduction.

The temperature-programmed desorption (TPD) measurements of NH_3 were carried out to examine acid properties of the catalysts surface. The measurements were accomplished with 0.300 g of a sample in the temperature range of 20–1000 °C, with helium as the carrier gas and NH_3 as the adsorbing gas. Prior to the measurement, each sample was calcined in helium at 500 °C, then cooled to 30 °C and an excess of NH_3 (ten doses, 840 μL each) was applied on the sample. Then, the sample was flushed with helium for 1 h to remove physically adsorbed ammonia and after that heating rate of 20 °C min^{-1} was applied. A change in NH_3 concentration was detected by the mass spectrometer Omnistar 300 (Pfeiffer Vacuum). During the experiments the following mass contributions *m*/*z* were collected: 2-H_2, 18-H_2O, and 16-NH_3.

The field-emission scanning electron microscopy (FE-SEM) images were taken using JSM-6700F scanning electron microscope. The samples for FE-SEM measurements were prepared by the powder depositing on a graphite tape.

Table 1
Physicochemical properties of investigated catalysts.

Catalyst	S_{BET} ($m^2\,g^{-1}$)	S_{meso} ($m^2\,g^{-1}$)	V_{micro} ($cm^3_{liq}\,g^{-1}$)	V_{total} ($cm^3_{liq}\,g^{-1}$)	H_2-TPR[a] (mmol g^{-1})	H_2-TPR[b] (mmol g^{-1})	H_2-TPR low-temperature peak maximum (°C)	NH_3-TPD[a] (mmol g^{-1})
CeZr	43	29	0.009	0.097	0.15	0.41	465	0.45
0.2Pt/CeZr	39	23	0.008	0.099	0.65	1.80	298	0.27
1.5Pt/CeZr	41	26	0.009	0.099	0.52	1.03	106	0.16
0.3Au/CeZr	39	24	0.008	0.100	0.55	1.10	415	0.31
2.8Au/CeZr	39	24	0.008	0.099	0.18	0.36	223	0.32

[a] Corresponding to total peak area between 25 and 500 °C.
[b] Corresponding to total peak area between 25 and 1000 °C.

2.3. Catalytic experiments

Dichloromethane and ethanol oxidations were carried out in a vertically placed fixed-bed tubular reactor made of quartz located in a ceramic tubular oven. The continuous flow reactor was operated under atmospheric pressure. The temperature of catalyst bed was measured on the reactor wall right before the catalyst bed. The catalytic activity tests were carried out with 0.870 g of fresh catalysts (grain size 0.16–0.32 mm) without any pretreatment. The inlet concentration of dichloromethane was 1000 volume ppm (~3.79 g m^{-3}) and the inlet concentration of ethanol was 1050 volume ppm (~2.11 g m^{-3}). The tests with dichloromethane were performed in the presence of 1.5 wt.% of water to ensure sufficient amount of hydrogen and thus improve the selectivity towards desired HCl [23–29]. Before the start of each catalytic test, the steady-state concentration of VOC in air stream was reached; with DCM after 20–35 min, with ethanol after 30–50 min. The flow of the reaction mixture was 1.03 L min^{-1}, which corresponded to the space velocity of 71 $m^3\,kg^{-1}\,h^{-1}$. The reaction temperature was linearly increased from 100 °C to 500 °C with heating rate 3.5 °C min^{-1} (DCM oxidation) and from 50 °C to 400 °C with the same heating rate (ethanol oxidation). Temperatures T_{50}, T_{90} and T_{95} (the temperature at which the 50%, 90% and 95% conversion of the VOC was observed, respectively) and the maximum conversion achieved during the experiment C_{max} were chosen as the measure of catalyst performance. The selectivity of the catalysts was judged in terms of the maximum concentration of CO_2 achieved during the experiment c_{max} (CO_2), the selectivity to CO_2 at 95 % conversion $S_{CD,95}$, the maximum selectivity to CO_2 achieved during the experiment $S_{CD,\,C_{max}}$, and the maximum HCl yield achieved during the experiment $Y_{HCl,max}$; details are shown in Ref. [24].

The gas measurement during the experiments was done with the Gasmet DX-4000N FTIR analyser. According to the manufacturer, the detection limit for the calibrated compounds is 2 ppm. The analyser was calibrated to detect chlorinated hydrocarbons (CH_2Cl_2, C_2Cl_4, C_2HCl_3, $CHCl_3$, CH_3Cl, $COCl_2$ and HCl) and oxy-derivatives of hydrocarbons (CO_2, CO, CH_3CHO, CH_2O, CH_3COOH, $CH_3COOC_2H_5$, CH_3OH, CH_3CH_2OH and C_2H_4). Due to the type of analysis, the formation of Cl_2 was not followed and the complete closing of chlorine balance was not possible.

3. Results and discussion

3.1. Catalysts characterization

This paper presents comprehensive investigation of dichloromethane and ethanol oxidation over a series of Pt and Au catalysts that were already tested in toluene and ethanol total oxidation [15]. Concerning chemical composition of catalysts, the XRF analysis confirmed that the weight ratio of Ce:Zr in the synthesized support is approximately 1:1. The catalysts were labelled according to actual contents of Au and Pt determined by ICP-AES analysis as 0.3Au/CeZr, 2.8Au/CeZr, 0.2Pt/CeZr, and 1.5Pt/CeZr.

Textural parameters of investigated catalysts determined from nitrogen physisorption measurements are listed in Table 1. It can be seen that all catalysts showed practically the same mesopore surface area, micropore volume and total pore volume. Thus, it may be stated that the deposition of Pt and Au and calcination of the catalysts after deposition of noble metals did not result in any substantial changes in the morphology of the porous structure of the catalysts. The typical nitrogen adsorption–desorption isotherm and the pore-size distribution of the investigated catalyst are shown in Fig. 1a and b. The shape of the nitrogen adsorption–desorption isotherm (Fig. 1a) corresponds to I + IV type isotherm according to IUPAC classification [30], which is typical for mesoporous materials with small portion of micropores. Moreover, the irregular hysteresis loop in a relatively broad range of relative pressures indicates the existence of bidisperse pore-size distribution, corresponding to the presence of smaller mesopores and some larger mesopores/macropores. These features pretty

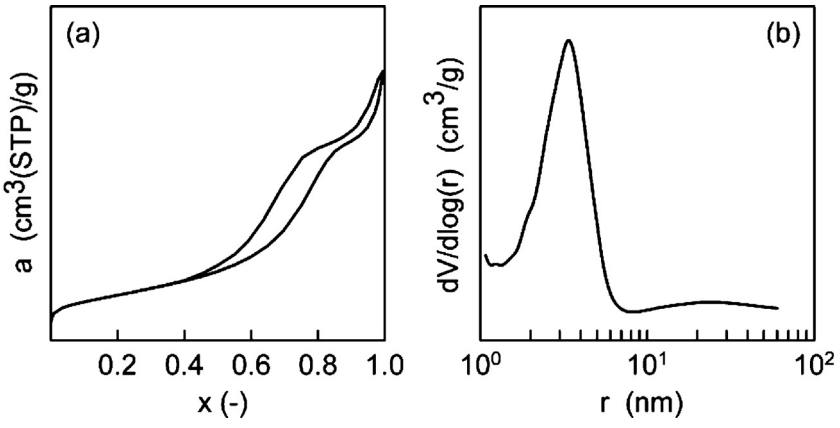

Fig. 1. Illustration of (a) the typical shape of nitrogen adsorption–desorption isotherm and (b) the pore-size distribution of the investigated catalysts.

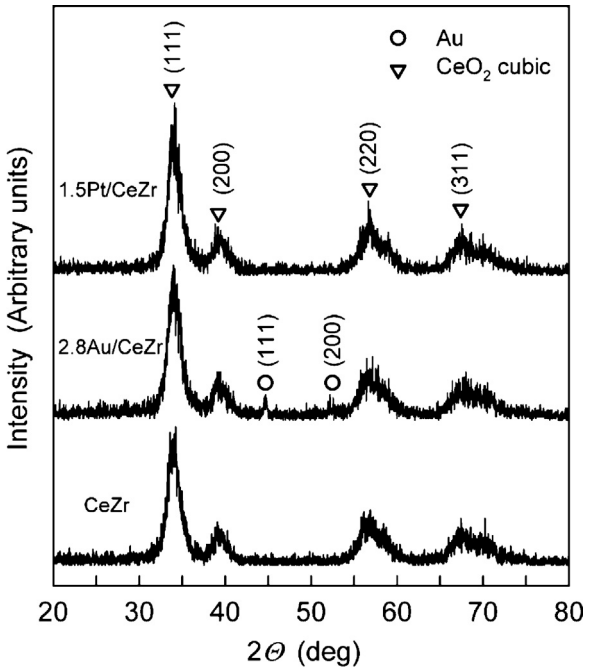

Fig. 2. XRD patterns of selected catalysts.

agree with the evaluated pore-size distribution (Fig. 1b). Besides the smaller mesopores showing the radius of ~3.4 nm, some larger mesopores/macropores are also seen.

X-ray powder diffraction patterns of the CeZr, 1.5Pt/CeZr and 2.8Au/CeZr catalysts are shown in Fig. 2. The diffraction lines at 34.1°, 39.0°, 56.7°, and 67.4° (2Θ) correspond to *h k l* reflections of cubic fluorite structure of CeO_2, however, they are slightly shifted to higher diffraction angels in comparison to regular *h k l* reflections of cubic CeO_2 (i.e. 33.3°, 38.6°, 55.7°, and 66.5°). Besides that, the diffraction lines of ZrO_2 crystalline phases are missing in XRD patterns. Both these features indicate that Zr ions are incorporated into the CeO_2 lattice, forming a ceria–zirconia solid solution (i.e. $Ce_{0.5}Zr_{0.5}O_2$) while maintaining its fluorite structure with cubic symmetry [31,32]. Based on the Scherrer equation, the crystallite size of CeZr was estimated to be 9 nm. For the 2.8Au/CeZr catalyst, other two diffraction lines at 44.8° and 52.3° (2Θ) can be seen, proving the presence of Au crystallites. The estimated Au mean crystallite size is 41 nm. The 1.5Pt/CeZr catalyst did not show any other diffraction lines except that from ceria–zirconia support. Thus, it can be stated that no crystalline Pt was detected on the catalyst surface by this method. In the XRD patterns of the 0.2Pt/CeZr and 0.3Au/CeZr catalysts (not shown in Fig. 2), no diffraction lines of noble metal crystallites can be distinguished due to low noble metal loadings.

The high similarity of textural parameters of all investigated catalysts corresponds to their similar crystallinity in respect to $Ce_{0.5}Zr_{0.5}O_2$ support. It is seen that the presence of Au crystallites did not markedly affect the porous structure of ceria–zirconia support.

The H_2-TPR profiles of the CeZr, Pt/CeZr and Au/CeZr catalysts are shown in Fig. 3. The CeZr catalyst showed two peaks centred at about 465 °C and 685 °C that can be assigned to the reduction of surface layer of ceria and bulk of ceria, respectively [33]. It is seen that the addition of platinum promoted the reduction of surface ceria. This effect can be ascribed to the hydrogen spillover from Pt particles onto the ceria–zirconia support [34]. With increasing platinum loading the reduction of surface ceria proceeded at lower temperatures. Similar behaviour was observed with gold catalysts,

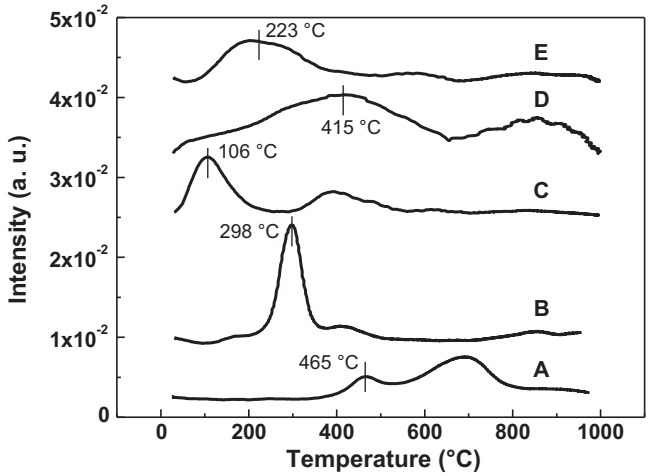

Fig. 3. H_2-TPR profiles of CeZr (A), 0.2Pt/CeZr (B), 1.5Pt/CeZr (C), 0.3Au/CeZr (D) and 2.8Au/CeZr (E).

although the promoting effect was less pronounced than in the case of platinum catalysts.

The NH_3-TPD profiles of the CeZr, Pt/CeZr and Au/CeZr catalysts are shown in Fig. 4. Desorption of ammonia proceeded in the temperature range from 25 to 500 °C. For the CeZr catalyst, a distinct desorption peak can be recognized at 123 °C with a shoulder at ~250 °C. It indicates that the catalyst possesses only acid sites of weak and medium strength. The surface species responsible for this acidity are coordinatively unsaturated Ce^{4+} and Zr^{4+} ions, which possess an uncompensated positive charge and create Lewis acidity [35]. From Table 1 it is seen that the introduction of both noble metals led to catalysts with decreased acidity in comparison with pristine ceria–zirconia. This decrease was more pronounced in the case of platinum catalysts.

3.2. Dichloromethane oxidation

The catalytic performance of examined catalysts in total oxidation of dichloromethane is shown in Table 2 and the light-off curves are depicted in Fig. 5. The catalytic performance was decreasing in the order CeZr > 0.2Pt/CeZr ~ 1.5Pt/CeZr ~ 0.3Au/CeZr > 2.8Au/CeZr (T_{90} was 467, 484, 485, 487 and 500 °C, respectively). Apart from high performance of CeZr support, it can be seen from Table 2 that also the maximum conversion of 98% was achieved with dichloromethane over the pure support material, whereas the

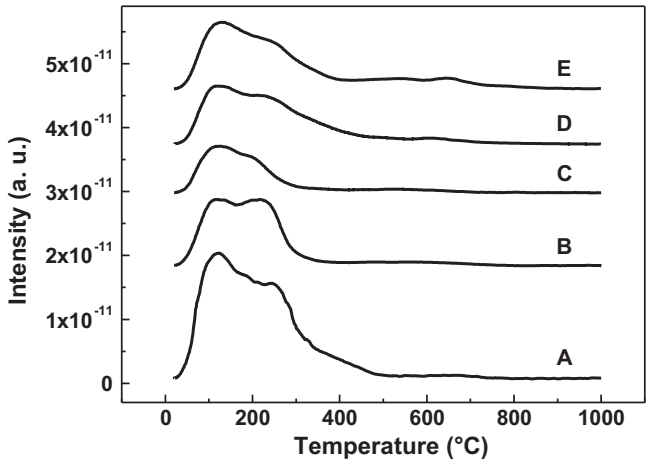

Fig. 4. NH_3-TPD profiles of CeZr (A), 0.2Pt/CeZr (B), 1.5Pt/CeZr (C), 0.3Au/CeZr (D) and 2.8Au/CeZr (E).

Table 2
Performance of catalysts in total oxidation of dichloromethane and ethanol.

Catalyst	Dichloromethane			Ethanol			
	T_{50} (°C)	T_{90} (°C)	C_{max} (%)	T_{50} (°C)	T_{90} (°C)	T_{95} (°C)	C_{max} (%)
CeZr	416	467	98	255	279	291	99
0.2Pt/CeZr	414	484	94	219	249	258	99
1.5Pt/CeZr	412	485	94	123	202	215	99
0.3Au/CeZr	417	487	94	257	270	274	99
2.8Au/CeZr	436	500	91	239	253	257	99

maximum conversions reached with Pt and Au catalysts were in the range from 91 to 94%. Hence, the introduction of noble metals on the ceria–zirconia mixed oxide led to decrease of its catalytic performance when the conversion of dichloromethane is considered. The influence of the noble metal loading was more pronounced with gold catalysts. While the Pt catalyst with higher loading of noble metal (1.5 wt.%) showed practically the same performance as the catalyst with lower loading (0.2 wt.%), the catalyst with lower Au loading (0.3 wt.%) was somewhat more active than the Au catalyst with 2.8 wt.% loading. It can be generally concluded that in our case the introduction of platinum or gold onto ceria–zirconia mixed oxide did not improve its catalytic performance when the conversion of dichloromethane is considered.

In the oxidation of dichloromethane, which can lead to the formation of by-products that are more toxic than the original compound, the selectivity is even more important than the performance [7]. 1.5 wt.% of water was added to the reaction mixture in order to ensure sufficient amount of hydrogen and thus improve the selectivity towards desired HCl [36], which can be easily removed by scrubbing the off-gasses. The maximum HCl yields over CeZr and all Pt and Au catalysts were comparable – varying from 73 to 77% (Table 3). Therefore it seems that the selectivity of Ce–Zr mixed oxide to HCl cannot be enhanced by depositing platinum or gold on ceria–zirconia mixed oxide.

The maximum concentrations of CO_2, CO and other detected by-products observed during dichloromethane oxidation are summarized in Tables 3 and 4. The maximum amount of CO_2 produced by the catalysts was practically the same for all noble metal catalysts (0.09–0.10 vol.%), while over the CeZr support only 0.05 vol.% of desired CO_2 was achieved. Concentration profiles of by-products for all tested catalyst are depicted in Fig. 6. Over the CeZr catalyst, only oxyderivatives of hydrocarbons were detected in addition to CO_2–605 ppm of CO and 4 ppm of CH_2O. Over the 1.5Pt/CeZr catalyst, only traces of CO and $CHCl_3$ were detected (up to 5 and 10 ppm, respectively). With decreased Pt loading (0.2Pt/CeZr) besides CO (17 ppm) and $CHCl_3$ (8 ppm) also traces of CH_2O (2 ppm) were identified. Over Au catalysts the produced amounts of CO were significantly higher than over Pt catalysts; lower concentrations of CO were observed with 2.8Au/CeZr (204 ppm) than with 0.3Au/CeZr (283 ppm). In addition to CO, traces of CH_2O (2–5 ppm) and $CHCl_3$ (7–12 ppm) were also detected. From Fig. 6 it is also clearly visible that over the Au catalysts chloroform was not produced until 430 °C (Fig. 6h and j), while over the Pt catalysts the formation of chloroform started at 310 °C (1.5Pt/CeZr) (Fig. 6f) and 407 °C (0.2Pt/CeZr) (Fig. 6d).

Based on the above mentioned results it can be seen that introduction of platinum on ceria–zirconia support significantly reduced the formation of undesired CO while enhancing the conversion to CO_2. In this respect, the highest selectivity to CO_2 was exhibited over 1.5Pt/CeZr catalyst followed by 0.2Pt/CeZr catalyst (the amount of undesired CO decreased from 605 ppm for CeZr catalyst to 4 ppm and 17 ppm for 1.5Pt/CeZr and 0.2Pt/CeZr catalysts, respectively). The positive effect of platinum on the decreased formation of undesired by-products was observed also in the case of formaldehyde. While with CeZr catalyst up to 4 ppm of CH_2O was observed, with 1.5Pt/CeZr the CH_2O formation was not detected at all and with 0.2Pt/CeZr the maximum concentration of CH_2O reached only 2 ppm. On the other hand, the introduction of platinum onto ceria–zirconia mixed oxide led to the formation of small amounts of chloroform, which was not detected at all with CeZr support alone (maximum detected concentration was 10 ppm with the 1.5Pt/CeZr catalyst).

In contrast to their platinum analogues, gold catalysts were generally less selective. However, they still exhibited lower formation of CO in comparison with the parent ceria–zirconia support (the maximum detected CO concentration decreased from 605 ppm for CeZr to 283 ppm with 0.3Au/CeZr and to 204 ppm with 2.8Au/CeZr). Whereas the maximum detected concentration of formaldehyde was comparable with CeZr support, varying from 3 to 5 ppm, the impregnation with gold led to the formation of chloroform (7–12 ppm), which was not detected with CeZr catalyst alone.

Gutiérez-Ortiz et al. [13] reported that both oxygen mobility and acidic properties are responsible for controlling the catalytic performance of the ceria–zirconia mixed oxide catalysts in the oxidation

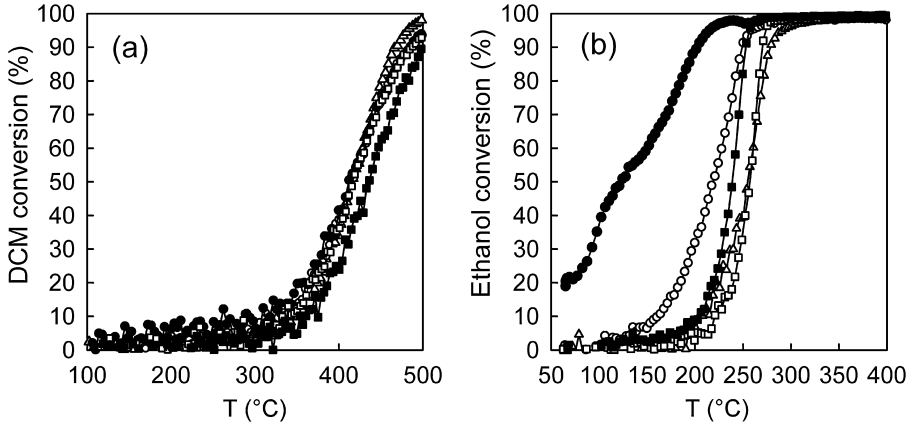

Fig. 5. Light-off curves for (a) dichloromethane oxidation and (b) ethanol oxidation: △: parent CeZr, ○: 0.2Pt/CeZr, ●: 1.5Pt/CeZr, □: 0.3Au/CeZr, ■: 2.8Au/CeZr.

Table 3
Selectivity of catalysts in total oxidation of dichloromethane and ethanol.

Catalyst	Dichloromethane		Ethanol	
	c_{max} (CO_2) (vol.%)	$Y_{HCl,max}$ (%)	$S_{CD,95}$ (%)	$S_{CD,\ cmax}$ (%)
CeZr	0.05	74	91	91
0.2Pt/CeZr	0.09	74	98	100
1.5Pt/CeZr	0.10	75	48	100
0.3Au/CeZr	0.09	77	98	100
2.8Au/CeZr	0.09	73	99	100

of chlorinated VOCs (1,2-dichloroethane and trichloroethylene). The hydrogen consumption during H_2-TPR of ceria–zirconia mixed oxide was shown to be proportional to the amount of reduced Ce^{4+} and thus also proportional to the amount of oxygen vacancies formed [37]. In our study, the introduction of platinum or gold on ceria–zirconia mixed oxide increased the reducibility of the catalysts. The total hydrogen consumption between 25 and 500 °C for the pristine CeZr support was 0.15 mmol g^{-1} while being 0.65 mmol g^{-1} for 0.2Pt/CeZr and 0.55 mmol g^{-1} for 0.3Au/CeZr catalysts, i.e. about four times higher. For 1.5Pt/CeZr, the total hydrogen consumption was 0.52 mmol g^{-1} and for 2.8Au/CeZr only 0.18 mmol g^{-1} (Table 1). Platinum introduction promoted the reduction of surface ceria and the increased Pt loading led to the shift of peak maxima to even lower temperature. Similar behaviour was observed with gold catalysts, nevertheless the promoting effect was less pronounced than in the case of platinum catalysts (Fig. 3). The obtained data indicate that noble metal itself did not significantly contribute to hydrogen consumption during the H_2-TPR experiment. Therefore, the increase in hydrogen consumption from 0.15 mmol g^{-1} for CeZr to ~0.5 mmol g^{-1} observed with 0.2Pt/CeZr, 1.5Pt/CeZr and 0.3Au/CeZr can be ascribed to the reduction of Ce^{4+} promoted by noble metal. Such promotion effects on the CeO_2 reducibility are well known for noble metals supported on ceria. For example, Yee et al. [38] showed by XPS studies that the addition of Pt partially reduces the CeO_2 surface. Similarly the catalytic activity of Au/CeO_2 was related to the capacity of gold nanoparticles to weaken the surface Ce—O bonds adjacent to Au atoms, thus enhancing the reactivity of the CeO_2 surface oxygen which is involved in the VOC oxidation through a Mars–van Krevelen reaction mechanism [39]. Moreover, it was shown that at temperatures higher than 300 °C gold is present just as Au^0 [40].

On the other hand, in our study the deposition of platinum or gold on ceria–zirconia mixed oxide led to a decrease of its acidity (Table 1). In general, the decrease in acidity was more significant for Pt catalysts and more pronounced with higher Pt loading. The investigated catalysts showed only Lewis acid sites of weak and medium strength (Fig. 4). Our NH_3-TPD results can be supported with some previous works [15,36,41]. It is well known that surface acid sites are catalytically active in the oxidation of dichloromethane [42–47]. However, Gutiérez-Ortiz et al. [13] proposed that the combination of surface acidity and accessible lattice oxygen controlled the catalytic performance of the Ce–Zr mixed oxides in the oxidation of C_2 chlorohydrocarbons. A similar conclusion – that optimal combination of surface acidity and redox property results in enhanced performance of catalyst in DCM oxidation – was also observed for Ce–Al mixed oxides [24,36,48].

Besides that it has been also reported that the oxidation of dichloromethane may be a structure sensitive reaction. In the case of platinum catalysts the reaction is promoted on a larger metallic particles and the catalytic performance is increasing with increasing density of reactive Pt–O species [29]. However, this is not the case with the gold catalysts. Their catalytic performance is higher when they possess rather small gold particles (<5 nm) [12,49,50]. Chen et al. [51] studied dichloromethane oxidation over Au/Co_3O_4 catalyst. They found out that the presence of highly dispersed small Au particles significantly increased the performance of the Co_3O_4 support. Nevertheless, for catalysts with similarly high Au dispersion the effect of gold loading (0.2–10 wt.%) on the catalytic performance was negligible.

In the present study, Ce–Zr supported catalysts with 0.2 wt.% and 1.5 wt.% of Pt exhibited very similar catalytic performance in dichloromethane oxidation. The same trend was also observed with 0.23 wt.% and 0.42 wt.% of Pt supported on Al_2O_3–CeO_2–zeolite in Ref. [29]. In contrary to platinum catalysts, the influence of particle size on the catalytic performance can be noticed with Au/CeZr catalysts. The differences in Au particle size for both investigated Au catalysts are illustrated in Fig. 7a–f. The lower catalytic performance of 2.8Au/CeZr compared to 0.3Au/CeZr can be attributed to the presence of larger Au particles with broad particle size distribution (Fig. 7c and f).

In conclusion, the decrease in acidity caused by doping of Ce–Zr support with gold or platinum is responsible for a lower catalytic performance of Pt/CeZr and Au/CeZr catalysts in the oxidation of dichloromethane despite the fact that the H_2-TPR profiles of 0.2Pt/CeZr, 1.5Pt/CeZr and 0.3Au/CeZr catalysts indicated that the presence of noble metals improves the reducibility of the surface Ce^{4+}. Besides that, the lower performance of Au catalysts is connected with the presence of poorly dispersed Au particles of relatively large size, which is in our study more pronounced for the catalyst with higher Au loading.

The acidity of the catalyst has been proposed to be a favourable property to promote the selectivity to HCl as well [49]. However, the lower acidity of Pt/CeZr and Au/CeZr catalysts did not lead to a considerable decrease of HCl yield in comparison with CeZr support (Table 3).

Table 4
Maximum concentrations of detected by-products in total oxidation of dichloromethane and ethanol.

Catalyst	Dichloromethane			Ethanol						
	CO (ppm)	CH_2O (ppm)	$CHCl_3$ (ppm)	CH_3CHO (ppm)	CH_2O (ppm)	CH_3OH (ppm)	CH_3COOH (ppm)	$CH_3COOC_2H_5$ (ppm)	C_2H_4 (ppm)	CO (ppm)
CeZr	605	4	n.d.	299	13	34	3	n.d.	14	292
0.2Pt/CeZr	17	2	8	440	9	8	2	n.d.	3	35
1.5Pt/CeZr	4	n.d.	10	581	6	n.d.	133	41	n.d.	n.d.
0.3Au/CeZr	283	5	7	285	12	33	3	2	n.d.	62
2.8Au/CeZr	204	3	12	314	8	19	n.d.	n.d.	n.d.	58

n.d., not detected; ppm, volume ppm.

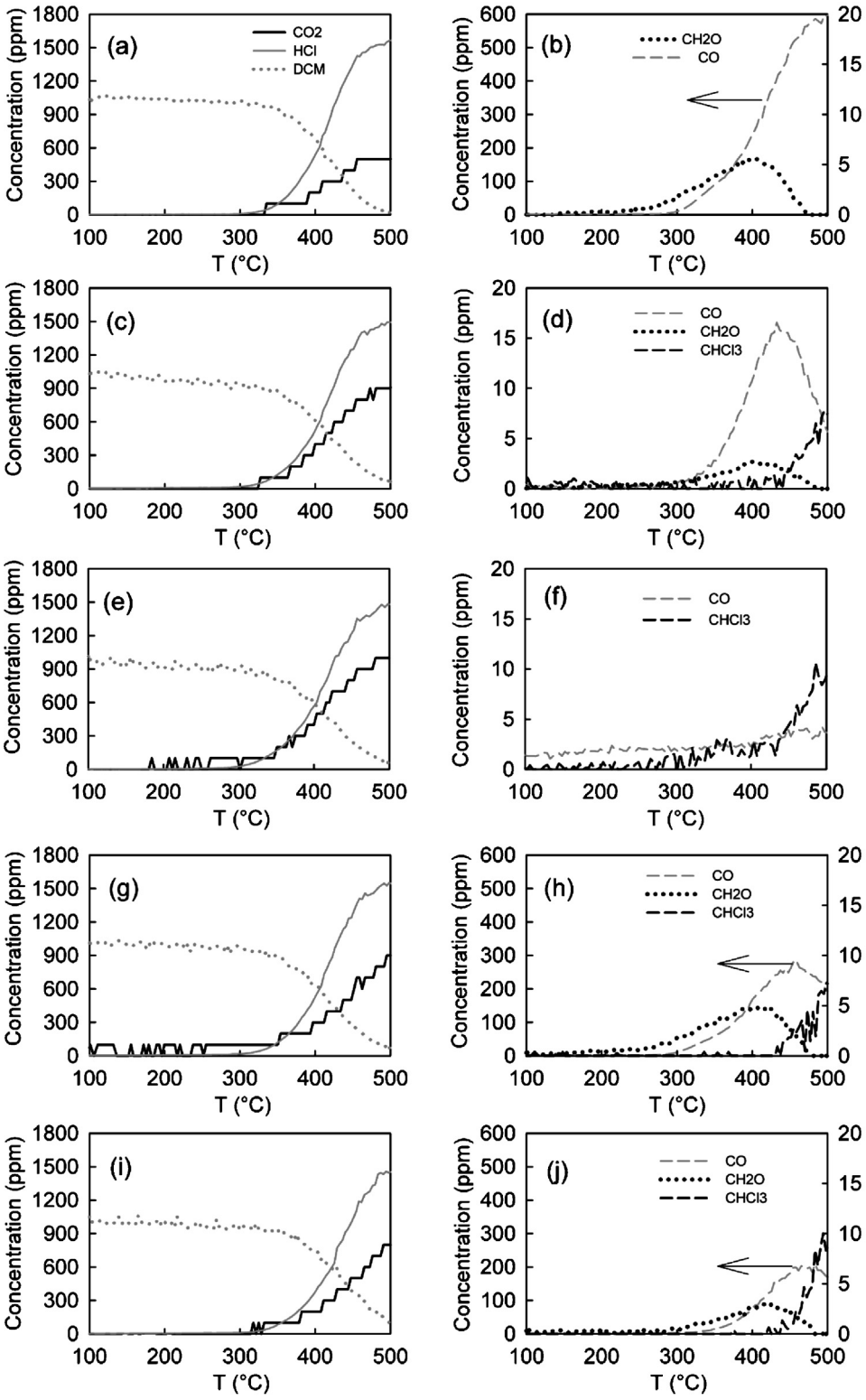

Fig. 6. Concentration profiles of dichloromethane and all detected by-products and products in dichloromethane oxidation; (a and b) parent CeZr, (c and d) 0.2Pt/CeZr, (e and f) 1.5Pt/CeZr, (g and h) 0.3Au/CeZr, (i and j) 2.8Au/CeZr. Dichloromethane concentration in air 1000 volume ppm, 1.5 wt.% of water, space velocity 71 $m^3\ kg^{-1}\ h^{-1}$, temperature range 100–500 °C, temperature ramp 3.5 °C min^{-1}, catalyst particle size 0.16–0.32 mm.

Concerning the formation of higher chlorinated by-products during dichloromethane oxidation, $CHCl_3$ formation was also observed over commercial catalysts 0.3Pt/Al_2O_3 (7714k, Katalevuna GmbH) [52] and 3.3Cu5.4Mn/Al_2O_3 (EnviCat® VOC-1544, Südchemie) [24], CuMn/ZrO_2–TiO_2–Al_2O_3 [53], Au/Co_3O_4 [51] or $LaCoO_3$ and $LaMnO_{3+\delta}$ perovskites [26]. In the case of perovskites the formation of higher chlorinated by-products ($CHCl_3$, CCl_4) in the temperature range 200–500 °C was related to the retention of chlorine atoms from transformed dichloromethane on the catalytic surface and this feature was more pronounced on $LaCoO_3$; adsorbed chlorine species further reacted with dichloromethane, which resulted in formation of chloroform and tetrachloromethane. In our

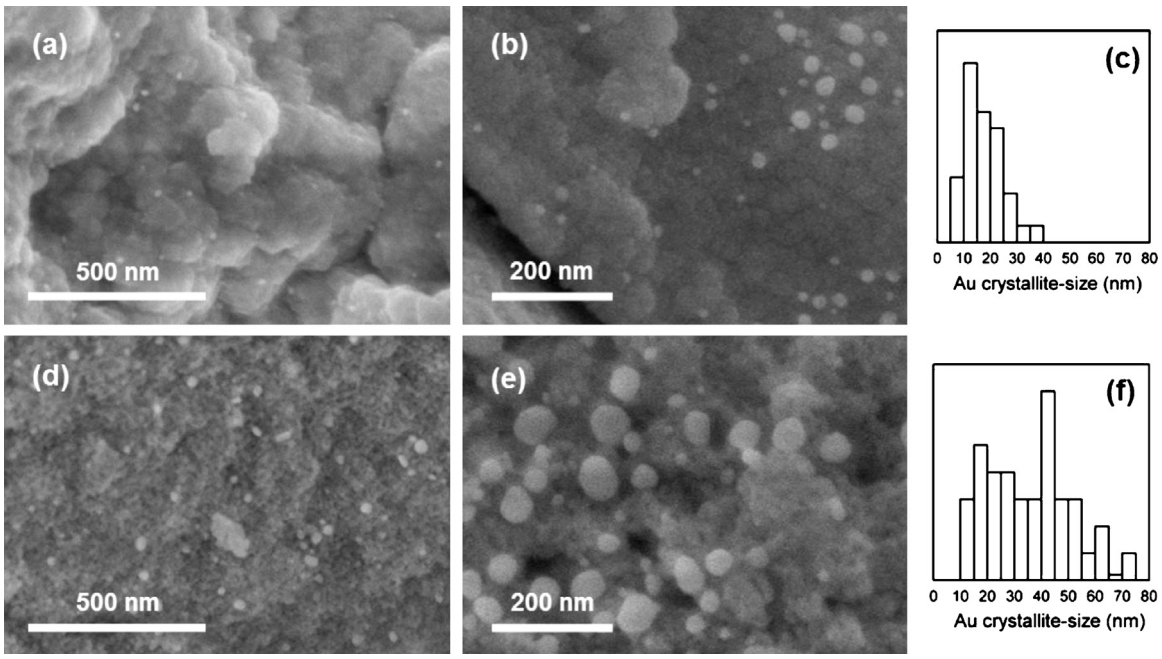

Fig. 7. FE-SEM images with Au crystallite-size distribution histograms of (a–c) 0.3Au/CeZr and (d–f) 2.8Au/CeZr.

study, based on the analysis of by-products formed over CeZr support and over Pt/CeZr and Au/CeZr catalysts (Table 4 and Fig. 6), it is obvious that noble metals (Pt, Au) play a key role in the formation of $CHCl_3$ over ceria–zirconia based catalysts and probably some chlorine species undergoing the reaction with dichloromethane are chemisorbed on noble metal active sites. However, chlorine atoms will originate either from transformed dichloromethane, or more probably from chlorine produced during Deacon reaction. This could explain higher temperatures of chloroform formation.

3.3. Ethanol oxidation

Temperatures of 50, 90 and 95% ethanol conversion are summarized in Table 2. The performance of the catalysts in total oxidation of ethanol decreased in the order of 1.5Pt/CeZr ≫ 0.2Pt/CeZr > 2.8Au/CeZr > 0.3Au/CeZr > CeZr as the T_{90} temperatures were 203, 249, 252, 270 and 279 °C, respectively. With the most efficient catalyst, 1.5Pt/CeZr, the 50% conversion of ethanol was achieved already at 123 °C, while for all other catalysts T_{50} was shifted to the temperatures by 95–130 °C higher. The decrease in the platinum loading from 1.5 to 0.2 wt.% led to a remarkable decrease of performance in the oxidation of ethanol (T_{50} for 0.2Pt/CeZr was 219 °C). The gold catalysts exhibited even lower performance, which for 0.3Au/CeZr was comparable to the Ce–Zr mixed oxide support (Table 2). Compared to the previous study [15] in which similar CeZr based catalysts were already examined in ethanol oxidation under different experimental conditions (i.e. using experimental apparatus with analysis of by-products by gas chromatograph with FID detector and Siemens Ultramat 23 IR analyser, GHSV 20 $m^3\ kg^{-1}\ h^{-1}$ and ethanol concentration 1 $g\ m^{-3}$), the same trend in catalytic performance of examined catalysts was observed.

From Table 2 and Fig. 5b it can be seen that the deposition of platinum on the Ce–Zr support resulted in the significant increase in the catalytic performance in ethanol oxidation, while the introduction of gold led to only minor enhancement. Similar trend in catalytic performance (Pt ≫ Au) was also observed by Santos et al. [54] who studied the total oxidation of ethanol over TiO_2 supported Au and Pt catalysts, even though their Au/TiO_2 catalysts contained much smaller gold nanoparticles (average diameter was 9 nm vs. ~20 and ~41 nm for 0.3Au/CeZr and 2.8Au/CeZr, respectively, in our case). In regard to Pt catalysts, they found that the intrinsic activity of Pt/TiO_2 catalysts in total oxidation of ethanol was doubled as the average particle size of platinum nanoparticles increased from 3.6 to 5.4 nm. Concerning Au catalysts, the slightly increased catalytic performance of 2.8Au/CeZr compared to 0.3Au/CeZr and practically comparable catalytic performance of 0.3Au/CeZr and CeZr indicates that for Au/CeZr catalysts with large Au particles (Fig. 7) the increase in Au particle size does not significantly affect the catalytic performance. This is not surprising for such large Au particles (~20 and ~41 nm for 0.3Au/CeZr and 2.8Au/CeZr, respectively). On the other hand, Santos et al. [54] showed that the light-off curve for Au/TiO_2 catalysts with gold particle size 4.0 nm was significantly shifted to lower temperatures in comparison with that for 9.1 nm, although their intrinsic activity was comparable (0.12 and 0.14 s^{-1}, respectively). Similarly, Fu et al. [55] who studied the water gas shift reaction on Au/CeO_2 reported that Au particle size is not a crucial factor influencing the catalytic performance. They concluded that in the water gas shift reaction the oxygen for the reaction is supplied by the ceria, thus, ceria particle size is very important, influencing the oxygen transfer. The presence of gold is important because CO adsorption takes place on gold. Fu et al. also showed that the catalytic performance of Au/CeO_2 in water gas shift reaction correlates with reducibility.

Concerning the selectivity of examined CeZr based catalysts in ethanol oxidation, all investigated noble metal supported catalysts exhibited higher selectivity to CO_2 than the pristine $Ce_{0.5}Zr_{0.5}O_2$ support (Table 3). While acetaldehyde and CO were the main by-products for the catalyst with low Pt loading and both Au catalysts, acetaldehyde, acetic acid and ethylacetate were the main by-products for the catalyst with high Pt loading (Fig. 8a–j and Table 4). Based on the distributions of reaction products (Fig. 8a–j) it is evident that over the 1.5Pt/CeZr catalyst a extensive oxidation of ethanol took place and relatively large amount of water was produced even at low temperatures. Moreover, in contrary to other investigated catalysts, no CO, C_2H_4 and CH_3OH were observed while increased formation of CO_2 appeared. The formation of acetic acid and ethylacetate in significant amounts (up to

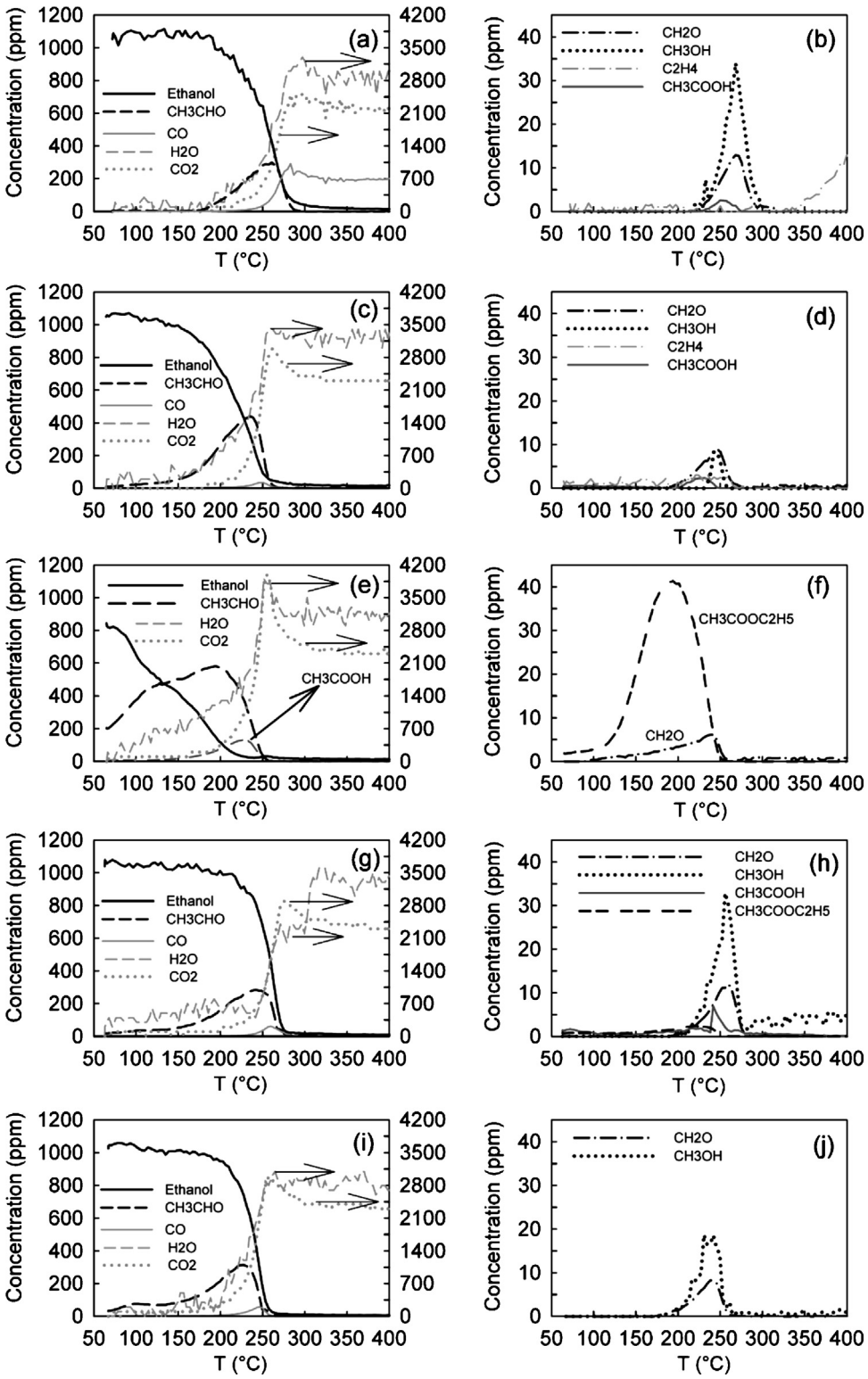

Fig. 8. Concentration profiles of ethanol and all detected by-products and products of ethanol oxidation: (a and b) parent CeZr, (c and d) 0.2Pt/CeZr, (e and f) 1.5Pt/CeZr, (g and h) 0.3Au/CeZr, (i and j) 2.8Au/CeZr. Ethanol concentration in air 1050 volume ppm, space velocity 71 $m^3\ kg^{-1}\ h^{-1}$, temperature range 70–400 °C, temperature ramp 3.5 °C min^{-1}, catalyst particle size 0.16–0.32 mm.

133 and 41 ppm, respectively) besides acetaldehyde indicates some important features, e.g. the influence of different nature of supported noble metals and different Pt loading on the performance of ceria–zirconia based catalyst in ethanol total oxidation. From comparison of concentration profiles of CeZr (Fig. 8a and b) and Pt/CeZr catalysts (Fig. 8c–f) it can be seen that the CeZr catalyst was less selective to CO_2 and relatively large amount of acetaldehyde and (subsequently by its oxidation) CO was produced. Besides that, traces of CH_3OH, CH_2O, acetic acid and ethylene were also detected. These compounds belong to products of acetaldehyde oxidation and/or decomposition. For example, traces of CH_3OH are formed by the reaction of produced CO and H_2 (which however cannot be

detected in our study by FTIR). Traces of ethylene formed at ~325 °C can be explained by dehydration of unreacted ethanol at higher temperatures. Over the 1.5Pt/CeZr catalyst, ethanol was oxidized through acetaldehyde selectively to CO_2. Practically only traces of CO (max. 35 ppm) were detected. In contrast to CeZr and 0.2Pt/CeZr, ethanol was adsorbed on the surface of the 1.5Pt/CeZr catalyst even at moderate temperature (~70 °C) and was oxidized trough acetaldehyde and acetic acid to CO_2, which was accompanied with the production of large amount of H_2O. Besides that, traces of ethyl acetate were detected (up to 41 ppm), which is formed by the reaction of acetic acid with ethanol. It is evident that the introduction of higher Pt loading enhanced the performance of the catalyst in ethanol oxidation and promoted the formation of acetic acid. The possible reaction pathways describing the formation of individual detected reaction by-products and products in ethanol oxidation are suggested in Eqs. (1)–(12).

$$CH_3CH_2OH + 3O_2 \rightarrow 2CO_2 + 3H_2O \quad (1)$$

$$CH_3CH_2OH + (1/2)O_2 \rightarrow CH_3CHO + H_2O \quad (2)$$

$$CH_3CHO + (1/2)O_2 \rightarrow CH_3COOH \quad (3)$$

$$CH_3CHO + (3/2)O_2 \rightarrow 2CO + 2H_2O \quad (4)$$

$$CH_3CHO \rightarrow 2CO + 2H_2 \text{ (via ketene species)} \quad (5)$$

$$CH_3COOH + 2O_2 \rightarrow 2CO_2 + 2H_2O \quad (6)$$

$$CH_3COOH + CH_3CH_2OH \rightarrow CH_3COOCH_2CH_3 + H_2O \quad (7)$$

$$CO + 2H_2 \rightarrow CH_3OH \text{ (in the presence of catalyst)} \quad (8)$$

$$CH_3OH + (1/2)O_2 \rightarrow CH_2O + H_2O \text{ (via formic acid)} \quad (9)$$

$$CH_2O + O_2 \rightarrow CO_2 + H_2O \quad (10)$$

$$CO + (1/2)O_2 \rightarrow CO_2 \quad (11)$$

$$CH_3CH_2OH \rightarrow C_2H_4 + H_2O \text{ (dehydration at higher temperature)} \quad (12)$$

By H_2-TPR measurements (Fig. 3) it was shown that the addition of Pt significantly promoted the reduction of surface ceria. With increasing Pt loading, the reduction of surface ceria proceeded at lower temperatures (Fig. 3, lines B and C). Our results correspond to several works [10,31,32,56] which reported that besides the increased reducibility of the $Ce_{0.5}Zr_{0.5}O_2$ catalysts due to oxygen vacancies resulting from the incorporation of ZrO_2 to CeO_2 lattice [31,32,56], Pt nanoparticles also trap and accumulate oxygen on their surface and perimeter sites and play the role of sites that contribute to oxidation of ethanol molecules and their partially oxidized derivatives to the final products [10]. The synergy between these two properties, which is evidently more pronounced at higher Pt loading, results in the observed phenomenon that the oxygen needed for the oxidation of adsorbed ethoxy species is provided more efficiently by such a catalyst, and as a consequence more acetic acid is produced during ethanol oxidation. This reaction mechanism influenced by catalyst redox properties was also reported by Mattos et al. [56] who studied ethanol oxidation over Pt catalysts supported on ZrO_2, Al_2O_3, CeO_2 and $Ce_{0.5}Zr_{0.5}O_2$ supports, de Lima et al. and Silva et al. [57–59] who studied decomposition, steam reforming, partial oxidation and oxidative steam reforming of ethanol over $CeZrO_2$ and $Pt/CeZrO_2$ catalysts using TPR-H_2, ethanol TPD and DRIFTS or Erdohelyi et al. [60] who examined interaction of ethanol and ethanol-water mixture with alumina- and ceria-supported noble metals.

Similarly to platinum, the introduction of gold on the $Ce_{0.5}Zr_{0.5}O_2$ support (Fig. 8g–j) increased the selectivity to CO_2. From comparison of the distributions of reaction products (Fig. 8c–j) it is obvious that the oxidation mechanism over both Au supported ceria–zirconia-based catalysts is similar to that of 0.2Pt/CeZr. The main reaction by-products were acetaldehyde and CO. Besides that, some CH_3OH and traces of CH_2O, acetic acid and ethylacetate were also detected, especially for 0.3Au/CeZr (Table 4). In contrast to 0.2Pt/CeZr, ethylene was not detected for any of the Au/CeZr catalysts. When compared to 0.2Pt/CrZr catalyst, for both Au catalysts the detected amounts of acetaldehyde were generally lower (285–314 ppm) and that of CO were slightly higher (58–62 ppm), indicating the ability of both gold catalysts to oxidize ethanol directly to CO and CO_2 (Tables 3 and 4, Fig. 8c, d and g–j). Moreover, the decreased amount of CH_3OH and absence of acetic acid and ethylacetate over 2.8Au/CeZr compared to 0.3Au/CeZr indicates that increased Au loading on ceria–zirconia support led to slightly higher selectivity to CO_2 at medium reaction temperatures (200–270 °C).

From the comparison of the distributions of reaction products over gold catalysts (Fig. 8g–j) it can also be seen that over both Au catalysts the ethanol oxidation took place already at low temperatures. However, over low Au loaded catalyst this process is more pronounced, resulting in lower detected amount of acetaldehyde accompanied with higher production of CO_2 and H_2O. The higher performance of 0.3Au/CeZr at low temperatures can be correlated with corresponding H_2-TPR patterns (Fig. 3, lines D and E). The reduction peak of surface ceria for 2.8Au/CeZr is shifted to lower temperatures (peak maximum at 223 °C) compared to 0.3Au/CeZr (peak maximum at 415 °C). On the other hand, the reduction peak of 0.3Au/CeZr is broader and its shoulder starts already at 25 °C, which correlates with enhanced catalytic performance of 0.3Au/CeZr at low temperatures. However, at higher temperatures (over 200 °C), the catalytic performance of 2.8Au/CeZr is superior to 0.3Au/CeZr, which explains the final order of catalytic performance 2.8Au/CeZr > 0.3Au/CeZr. In addition, the generally lower catalytic performance of gold catalysts may be connected also to the lower ability of this metal to dissociatively chemisorb oxygen [54].

4. Conclusions

Ceria–zirconia mixed oxide ($Ce_{0.5}Zr_{0.5}O_2$) prepared by sol–gel method was impregnated with gold(III) acetate or platinum(II) tetraaminehydroxide, characterized and tested as a catalyst for total oxidation of dichloromethane and ethanol in air.

It was shown that from the viewpoint of porous structure all catalysts are very similar and the deposition of different loadings of both noble metals did not result in any significant changes of porous structure of the catalysts. The deposition of platinum and gold on $Ce_{0.5}Zr_{0.5}O_2$ support enhanced the reducibility of surface ceria. With increasing platinum loading, the reduction of surface ceria proceeded at lower temperatures. Similar behaviour was observed with gold catalysts, although the promoting effect of noble metal was less pronounced. Introduction of both noble metals led to the catalysts with decreased acidity in comparison with the $Ce_{0.5}Zr_{0.5}O_2$ support. This decrease was more pronounced in the case of platinum catalysts.

In total oxidation of dichloromethane, the catalytic performance of pristine $Ce_{0.5}Zr_{0.5}O_2$ was slightly better than that of platinum and gold catalysts supported on the same mixed oxide. This can be attributed to lower amount of acid sites that act as chemisorption sites for chlorinated compounds. On the other hand, platinum

catalysts exhibited significantly enhanced selectivity to CO_2 in comparison with the $Ce_{0.5}Zr_{0.5}O_2$ support. The main reaction by-product in dichloromethane oxidation was CO together with traces of CH_2O. Small amount of chloroform (up to 10 ppm) was also detected over all noble metal catalysts. Gold catalysts were generally less selective than their platinum analogues.

In total oxidation of ethanol, the deposition of platinum on the $Ce_{0.5}Zr_{0.5}O_2$ support resulted in a significantly increased catalytic performance, while the introduction of gold led to only minor enhancement. The positive effect of higher noble metal loading on catalytic performance was more pronounced for Pt catalysts. For all investigated catalysts, the position of the H_2-TPR peak corresponding to the reduction of surface ceria correlated with their catalytic performance. Both platinum and gold catalysts exhibited higher selectivity to CO_2 than the pristine $Ce_{0.5}Zr_{0.5}O_2$. The influence of Pt loading on mechanism of ethanol oxidation was revealed, while this was not the case with gold. Acetaldehyde and CO were the main by-products for low Pt loading and both Au catalysts, while acetaldehyde, acetic acid and ethylacetate were found with the catalyst having high Pt loading. This can be attributed to the synergistic effects of platinum nanoparticles, which increased the reducibility of the support but also formed the active sites for the oxidation reaction. Based on concentration profiles of individual by-products/products detected by on-line FTIR analysis, the possible pathways of their formation were suggested.

Acknowledgements

The financial support of the Grant Agency of the Czech Republic (Project 13-24186P) is gratefully acknowledged. The authors thank Dr. Jan Procházka from the J. Heyrovský Institute of Physical Chemistry of the ASCR, v.v.i. for FE-SEM images.

References

[1] R. Atkinson, Atmospheric Environment 34 (2000) 2063–2101.
[2] R.G. Derwent, M.E. Jenkin, S.M. Saunders, M.J. Pilling, P.G. Simmonds, N.R. Passant, G.J. Dollard, P. Dumitrean, A. Kent, Atmospheric Environment 37 (2003) 1983–1991.
[3] A. Casset, F. De Blay, Revue des Maladies Respiratoires 25 (2008) 475–485.
[4] http://www.eurochlor.org/chlorinated-solvents-%28ecsa%29/facts-figures.aspx
[5] International Chemical Safety Cards, http://www.cdc.gov/niosh/ipcsneng/neng0058.html
[6] P. Hunter, S.T. Oyama, Control of Volatile Organic Compound Emissions, John Wiley, New York, 2000.
[7] S. Ojala, S. Pitkäaho, T. Laitinen, N.N. Koivikko, R. Brahmi, J. Gaálová, L. Matějová, A. Kucherov, S. Paivarinta, C. Hirschmann, T. Nevanpera, M. Riihimaki, M. Pirila, R.L. Keiski, Topics in Catalysis 54 (2011) 1224–1256.
[8] F.I. Khan, A.K. Ghoshal, Journal of Loss Prevention in the Process Industries 13 (2000) 527–545.
[9] L.F. Liotta, Applied Catalysis B 100 (2010) 403–412.
[10] L.M. Petkovic, S.N. Rashkeev, D.M. Ginosar, Catalysis Today 147 (2009) 107–114.
[11] S. Pitkäaho, S. Ojala, T. Kinnunen, R. Silvonen, R.L. Keiski, Topics in Catalysis 54 (2011) 1257–1265.
[12] S. Scire, L.F. Liotta, Applied Catalysis B 125 (2012) 222–246.
[13] J.I. Gutiérrez-Ortiz, B. de Rivas, R. López-Fonseca, J.R. González-Velasco, Applied Catalysis A 269 (2004) 147–155.
[14] J.I. Gutierrez-Ortiz, B. de Rivas, R. Lopez-Fonseca, J.R. Gonzalez-Velasco, Applied Catalysis B 65 (2006) 191–200.
[15] J. Gaálová, P. Topka, L. Kaluža, O. Šolcová, Catalysis Today 175 (2011) 231–237.
[16] S. Brunauer, P.H. Emmett, E. Teller, Journal of the American Chemical Society 60 (1938) 309–319.
[17] J.H. Deboer, B.C. Lippens, B.G. Linsen, J.c. Broekhof, A. Vandenhe, T.J. Osinga, Journal of Colloid and Interface Science 21 (1966) 405.
[18] P. Schneider, Applied Catalysis A 129 (1995) 157–165.
[19] E.P. Barrett, L.G. Joyner, P.P. Halenda, Journal of the American Chemical Society 73 (1951) 373–380.
[20] B.F. Roberts, Journal of Colloid and Interface Science 23 (1967) 266.
[21] A. Lecloux, J.P. Pirard, Journal of Colloid and Interface Science 70 (1979) 265–281.
[22] P. Scherrer, Göttinger Nachrichten Gesell. 2 (1918) 98–100.
[23] K. Everaert, J. Baeyens, Journal of Hazardous Materials 109 (2004) 113–139.
[24] L. Matějová, P. Topka, K. Jirátová, O. Šolcová, Applied Catalysis A: General 443–444 (2012) 40–49.
[25] R. López-Fonseca, J.I. Gutiérrez-Ortiz, J.R. González-Velasco, Catalysis Communications 5 (2004) 391–396.
[26] G. Sinquin, C. Petit, S. Libs, J.P. Hindermann, A. Kiennemann, Applied Catalysis B 27 (2000) 105–115.
[27] R. Lopez-Fonseca, S. Cibrian, J.I. Gutierrez-Ortiz, M.A. Gutierrez-Ortiz, J.R. Gonzalez-Velasco, AIChE Journal 49 (2003) 496–504.
[28] J.R. Gonzalez-Velasco, A. Aranzabal, R. Lopez-Fonseca, R. Ferret, J.A. Gonzalez-Marcos, Applied Catalysis B 24 (2000) 33–43.
[29] S. Pitkäaho, S. Ojala, T. Maunula, A. Savimäki, T. Kinnunen, R.L. Keiski, Applied Catalysis B 102 (2011) 395–403.
[30] S.J. Gregg, K.S.W. Sing, Adsorption, in: Surface Area and Porosity, Academic Press, New York, 1982.
[31] J. Kašpar, P. Fornasiero, M. Graziani, Catalysis Today 50 (1999) 285–298.
[32] M.H. Yao, R.J. Baird, F.W. Kunz, T.E. Hoost, Journal of Catalysis 166 (1997) 67–74.
[33] L.F. Liotta, A. Longo, G. Pantaleo, G. Di Carlo, A. Martorana, S. Cimino, G. Russo, G. Deganello, Applied Catalysis B 90 (2009) 470–477.
[34] L.V. Mattos, F.B. Noronha, Journal of Power Sources 145 (2005) 10–15.
[35] B. de Rivas, R. López-Fonseca, M.A. Gutiérrez-Ortiz, J.I. Gutiérrez-Ortiz, Applied Catalysis B 104 (2011) 373–381.
[36] S. Pitkäaho, T. Nevanperä, L. Matějová, S. Ojala, R.L. Keiski, Applied Catalysis B 138–139 (2013) 33–42.
[37] G. Balducci, J. Kašpar, P. Fornasiero, M. Graziani, M.S. Islam, J.D. Gale, Journal of Physical Chemistry B 101 (1997) 1750–1753.
[38] A. Yee, S.J. Morrison, H. Idriss, Journal of Catalysis 191 (2000) 30–45.
[39] S. Scirè, S. Minicò, C. Crisafulli, C. Satriano, A. Pistone, Applied Catalysis B 40 (2003) 43–49.
[40] E.D. Park, J.S. Lee, Journal of Catalysis 186 (1999) 1–11.
[41] S. Pitkäaho, L. Matejova, K. Jiratova, S. Ojala, R.L. Keiski, Applied Catalysis B 126 (2012) 215–224.
[42] G.C. Bond, R.C. Francisco, Catalysis Letters 39 (1996) 261–263.
[43] R.W. van den Brink, P. Mulder, R. Louw, G. Sinquin, C. Petit, J.P. Hindermann, Journal of Catalysis 180 (1998) 153–160.
[44] I. Maupin, L. Pinard, J. Mijoin, P. Magnoux, Journal of Catalysis 291 (2012) 104–109.
[45] H. Windawi, Z.C. Zhang, Catalysis Today 33 (1997) 411.
[46] J. Haber, T. Machej, M. Derewinski, R. Janik, J. Krysciak, H. Sadowska, J. Janas, Catalysis Today 54 (1999) 47–55.
[47] R.H. Ma, P.J. Hu, L.Y. Jin, Y.J. Wang, J.Q. Lu, M.F. Luo, Catalysis Today 175 (2011) 598–602.
[48] Q.Y. Chen, N. Li, M.F. Luo, J.Q. Lu, Applied Catalysis B 127 (2012) 159–166.
[49] R. López-Fonseca, J.I. Gutiérrez-Ortiz, J.L. Ayastui, M.A. Gutiérrez-Ortiz, J.R. González-Velasco, Applied Catalysis B 45 (2003) 13–21.
[50] M. Haruta, Catalysis Today 36 (1997) 153–166.
[51] B.S. Chen, C.S. Bai, R. Cook, J. Wright, C. Wang, Catalysis Today 30 (1996) 15–20.
[52] J. Corella, J.M. Toledo, A.M. Padilla, Applied Catalysis B 27 (2000) 243–256.
[53] Y. Gu, Y. Yang, Y. Qiu, K. Sun, X. Xu, Catalysis Communications 12 (2010) 277–281.
[54] V.P. Santos, S.A.C. Carabineiro, P.B. Tavares, M.F.R. Pereira, J.J.M. Órfão, J.L. Figueiredo, Applied Catalysis B 99 (2010) 198–205.
[55] Q. Fu, A. Weber, M. Flytzani-Stephanopoulos, Catalysis Letters 77 (2001) 87–95.
[56] L.V. Mattos, F.B. Noronha, Journal of Power Sources 152 (2005) 50–59.
[57] S.M. de Lima, I.O. da Cruz, G. Jacobs, B.H. Davis, L.V. Mattos, F.B. Noronha, Journal of Catalysis 257 (2008) 356–368.
[58] S.M. de Lima, A.M. Silva, U.M. Graham, G. Jacobs, B.H. Davis, L.V. Mattos, F.B. Noronha, Applied Catalysis A 352 (2009) 95–113.
[59] A.M. Silva, L.O.O. Costa, A. Barandas, L.E.P. Borges, L.V. Mattos, F.B. Noronha, Catalysis Today 133 (2008) 755–761.
[60] A. Erdohelyi, J. Rasko, T. Kecskes, M. Toth, M. Domok, K. Baan, Catalysis Today 116 (2006) 367–376.